Received: 8 August 2025 | Revised: 17 September 2025 | Accepted: 16 October 2025 | Published online: 31 October 2025

RESEARCH ARTICLE

Smart Wearable Technology
2025, Vol. 00(00) 1–7
DOI: 10.47852/bonviewSWT52027122

BON VIEW PUBLISHING

Dynamic THz Hologram Generation via Temperature-Tunable Aerogel-Spacer Graphene Metasurfaces for Sensing Applications

Alireza Barati Haghverdi[1], Amir Ali Mohammad Khani[2], Ilghar Rezaei[3], Ali Soldoozy[4] and Toktam Aghaee[5,*]

[1]*Department of Civil Engineering, Asrar Institute of Higher Education of Mashhad, Iran*

[2]*Department of Electrical Engineering, Sav.C., Islamic Azad University, Iran*

[3]*Department of Electrical Engineering, CT.C., Islamic Azad University, Iran*

[4]*Department of Electrical Engineering, Ya.C., Islamic Azad University, Iran*

[5]*Department of Electrical Engineering, Semnan University, Iran*

Abstract: Metasurfaces, as two-dimensional artificial materials, have revolutionized optics by enabling unprecedented control over light propagation, with profound implications for sensing, encryption, displays, and computational imaging. This research presents the modeling and design of a circuit-based metasurface engineered to dynamically generate holographic images within the terahertz (THz) spectrum, thereby expanding the horizon of practical technological applications. The proposed methodology employs an equivalent circuit model, grounded in transmission line theory, to represent the THz metasurface. This innovative approach effectively reduces complex electromagnetic interactions into discrete circuit components, facilitating a highly efficient and intuitive analysis of key performance metrics such as reflection magnitude and phase shift. A genetic algorithm was subsequently deployed to optimize the critical unit cell parameters including the dimensions of the graphene ribbons, their periodicity, and the thickness of the dielectric spacer to achieve a full 2π phase coverage at the target operational frequency of 0.8 THz, a prerequisite for high-fidelity hologram generation. Crucially, the dynamic reconfiguration of the generated THz holograms is enabled by the integration of temperature-sensitive aerogels, which modulate the metasurface's optical response. The outcomes of this optimization are validated through full-wave electromagnetic simulations, which confirm enhanced operational efficiency and remarkable flexibility. This work underscores the potent synergy of circuit modeling and metasurface technology, paving the way for scalable, cost-effective, and high-performance active THz devices for next-generation communication and imaging systems.

Keywords: THz metasurfaces, circuit modeling, aerogels, dynamic holography, transmission line method

1. Introduction

Metasurfaces, sub-wavelength structures with a strong capability to manipulate light properties such as amplitude, phase, polarization, and the direction of propagation, have revolutionized the field of optics by introducing phase discontinuity in the light propagation and flat optics rather than traditional bulky optics [1, 2].

Holography, as an emerging technique that captures and reconstructs the light field emitted by an object, has found applications in various fields including imaging, medical imaging, and data encryption [3–5]. These applications are highly promising in the terahertz (THz) region of electromagnetic waves [6–8]. This comes from the fact that THz gap capability has not yet been explored. Hence, developing THz structures capable of generating reconfigurable holograms is highly promising and in demand.

This work presents a novel thermally tunable THz metasurface for dynamic holography, uniquely incorporating temperature-sensitive aerogel spacers with graphene ribbons and optimized via an efficient equivalent circuit model validated by full-wave simulations. While [9, 10] predominantly use phase-change materials or spin-multiplexing with electrical or optical modulation, the proposed design leverages thermal modulation of aerogel thickness for low-power, fabrication-compatible tuning. The chosen dimensions and materials are carefully optimized to achieve full 2π phase control at 0.8 THz and align well with or improve upon reported scales.

This study introduces an innovative strategy for fabricating dynamic THz holograms through the integration of metasurfaces with temperature-responsive aerogels, employing circuit-theoretic modeling approaches. Initially, we elucidate the fundamental theoretical principles governing THz metasurfaces alongside the modulatory influence of aerogels on their electromagnetic characteristics. Subsequently, we outline the circuit model framework utilized to simulate and optimize the metasurface

*Corresponding author: Toktam Aghaee, Department of Electrical Engineering, Semnan University, Iran. Email: Toktam.Aghaee@semnan.ac.ir

functionality. Validation is conducted leveraging Finite Difference Time Domain (FDTD) simulations [11, 12], affirming the feasibility and efficacy of the proposed methodology.

The core problem addressed is the design and modeling of a dynamically tunable THz metasurface capable of generating reconfigurable holograms via temperature-induced modulation of a dielectric spacer's thickness integrated with graphene elements, which enables real-time control over amplitude and phase of reflected THz waves at 0.8 THz. The primary challenge lies in developing a scalable, cost-effective design and optimization methodology that accurately predicts the electromagnetic response of such metasurfaces while reducing computational complexity. We solve this by introducing an equivalent circuit model (ECM) approach based on transmission line theory combined with a genetic algorithm for parameter optimization. This work particularly focuses on leveraging temperature-sensitive aerogels as tunable spacers, a novel mechanism distinct from common phase-change materials, demonstrating two-state hologram generation validated through full-wave simulations.

2. Design

The schematic representation of the designed THz metasurface unit cell is depicted in Figure 1(a). The structure operates in reflection mode and incorporates a thick gold layer as the substrate, an aerogel dielectric spacer serving as the tunable element, and a graphene ribbon positioned on top. However, generating dynamic holograms by dynamically altering the thickness of the dielectric spacer has not been explored.

Simulation points were used to discretize the phase into 12 levels. The embedded graphene ribbon represents the orientation shift.

The tunability of the described structure is controlled by temperature-induced changes in the dielectric spacer, rather than by adjusting the graphene's Fermi level through a DC voltage, as shown in Figure 1(b). However, modifying the graphene's chemical potential (or Fermi level) electrically offers more versatile control over the manipulation of THz waves. By applying different gate voltages, the graphene's conductivity and chemical potential can be actively tuned, which in turn allows independent modulation of both the amplitude and phase of the reflected THz waves. This electrical tuning provides a flexible and efficient means to dynamically control THz beam properties, enabling advanced applications such as beam shaping, sensing, and communication systems.

While the electrical tuning of graphene enables flexible dynamic control of THz beam properties and advanced

Figure 1

(a) Schematic of the unit cell design forming the basis of the proposed THz metasurface, (b) tunability mainly achieved by adjusting dielectric spacer thickness via temperature – graphene Fermi level tuning was held constant in main hologram demonstrations, (c) circuit modeling based on the transmission line method, and (d) amplitude and phase profiles using Pancharatnum–Berry technique at 0.8 THz

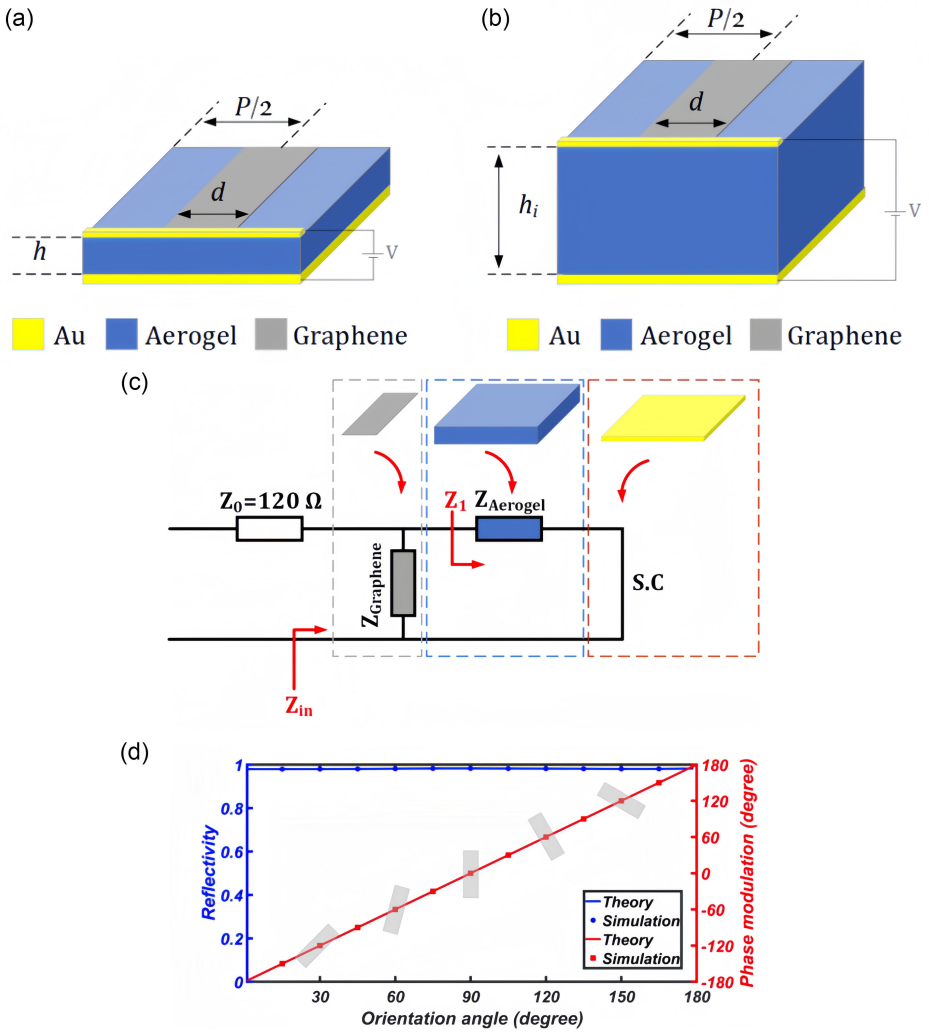

applications (beam shaping, sensing, communication), it is acknowledged that this discussion appears somewhat detached from the core focus of the presented structure, which primarily achieves dynamic hologram tuning via temperature-induced changes in the dielectric spacer thickness. While electrical control of graphene's Fermi level is mentioned as a known, promising mechanism in literature, it is not actively exploited in the simulations [13, 14].

To design the proposed metasurface capable of dynamic phase modulation, we utilized a genetic algorithm along with circuit modeling of the elements based on the transmission line method in the THz spectrum, as illustrated in Figure 1(c).

The electrical conductivity of graphene in the THz band is primarily described by its intra-band conductivity, which results from intra-band electron transitions. This intra-band conductivity can be accurately modeled using the Drude model as Equation (1) [11].

$$\sigma(\omega)_{\text{intra}} = -\frac{je^2 K_B T}{\pi\hbar^2(\omega - 2j\Gamma)}\left(\frac{\mu_c}{K_B T} + 2ln\left(\frac{1}{e^{\frac{\mu_c}{K_B T}} + 1}\right)\right) \quad (1)$$

where KB is the Boltzmann constant, T is the temperature, μc is the graphene Fermi level, $\hbar$ is the reduced Planck constant, Γ is the scattering rate of electrons, and τ is the electron relaxation time.

The effect of temperature change on the graphene Fermi level in the THz regime that this device is designed for is not significant and can be calculated using Equation (1). Hence, we did not consider this effect in our design.

In this regard, Figure 2 is shown to highlight the negligible effects of temperature on the graphene conductivity.

Furthermore, the graphene electrical permittivity is described by Equation (2) [11].

$$\varepsilon = 1 + j\frac{\sigma}{\omega.\varepsilon_0.t} \quad (2)$$

In which σ is the electrical conductivity of graphene, t is the graphene thickness and consider 1 nm (equal to 3 atom carbons), ε_0 free space electrical permittivity, angular frequency.

The consideration of minor effects such as coupling between layers and the influence of graphene wires in the ECM can indeed enhance its accuracy and reliability in simulating graphene-based THz devices. Incorporating these subtle phenomena makes the ECM more representative of the actual physical behavior, resulting in more robust and precise predictions [15, 16].

However, it is important to balance the level of detail with computational efficiency. As the ECM gains complexity by including more interaction effects, the number of variables and possible scenarios to explore increases significantly. This places higher demands on computing resources like CPU power and memory (RAM), which can limit the speed and practicality of simulations, especially when hardware capabilities are constrained.

The ECM of graphene ribbons is described by Equation (3) [11]. Furthermore, Table 1 summarizes constants, and Table 2 tabulates eigenvalues.

$$\begin{aligned} R_n &= \frac{D}{S_n^2}\frac{\pi\hbar^2}{e^2 E_F \tau} \\ L_n &= \frac{D}{S_n^2}\frac{\pi\hbar^2}{e^2 E_F} = R_n \tau \\ C_n &= \frac{S_n^2}{D}\frac{2\varepsilon_{\text{eff}}}{q_n} \end{aligned} \quad (3)$$

where R_n, L_n, and C_n are the equivalent resistance, inductor, and capacitor of the series branch. Additionally, ε_{eff} is the effective

Figure 2
Graphene conductivity counterparts versus different temperatures

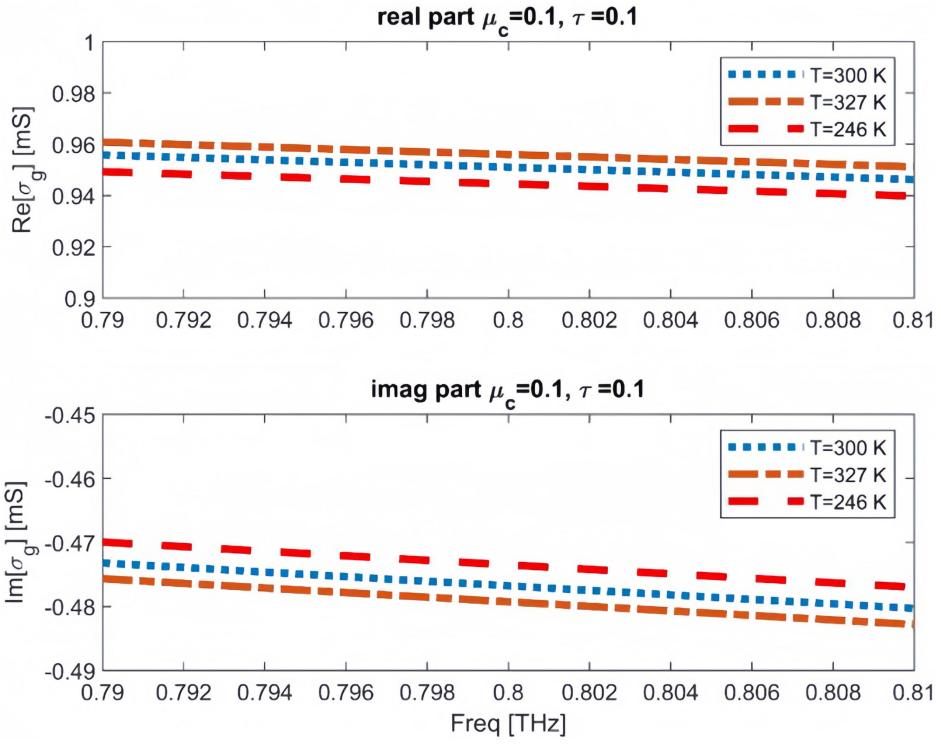

Table 1
Constant parameters

$\tau = 0.1\text{pS}$ and $\Gamma = \frac{1}{\tau}$	KB = 1.3806288 × 10−23 J.K-1
$\varepsilon_{\text{eff}} = \frac{\varepsilon_1+\varepsilon_2}{2} = \frac{n_1{}^2\varepsilon_0+n_2{}^2\varepsilon_0}{2}$	T = 300° K
$\varepsilon_0 = \frac{1}{\mu_0 v_0{}^2} \rightarrow \upsilon_0 = \frac{1}{\sqrt{\varepsilon_0\mu_0}} = 3 \times 10^8 \frac{\text{m}}{\text{s}}$	e = 1.602 × 10−19 C
Disk: $q_{11} = \frac{0.472}{a}, S_1 = 0.6087a, K_1 = 1.2937$	Z0 = 120 πΩ
Ribbon: $q_1 = \frac{\pi}{W} \times 0.51, S_1 = 0.0037$	EF = eμc
$\eta = \sqrt{\frac{\mu_0}{\varepsilon_0}} = \sqrt{\frac{4\pi \times 10^{-7}}{8.85 \times 10^{-12}}} = 376.8194$	0 eV < μc < 1 eV
$\varepsilon_0 = 8.85 \times 10^{-12} \frac{\text{F}}{\text{m}}$	0.1 THz < f < 10 THz
$Z_d = \frac{\eta}{n_d} = \frac{Z_0}{n_d} = \frac{376.8194}{1.53} = \frac{120\pi}{1.53} = 246.2872$	□ = 2πf
$\hbar = \frac{h}{2\pi} = \frac{6.626068 \times 10^{-34}\text{J.S}}{2\pi} = 1.054572 \times 10^{-34}\text{J.S} = 6.58 \times 10^{-16}\text{eVs}$	

Table 2
The value of q_n and based on the geometry of the proposed device

$\frac{W}{D}$	0.1	0.3	0.5	0.7	0.9
for Graphene Ribbons: $q_1 \frac{W}{\pi}$	0.734	0.710	0.658	0.571	0.420

permittivity, and ε_0 is the free space permittivity. So, D is the period of ribbons, is the reduced Planck constant, and q_n is the eigenvalue and is expressed in Table 2.

To obtain q_n, physical parameters, such as a, L, W, and D, must be designed and then referred to Table 2 [11].

Understanding the ECM for each component allows us to represent device performance using a nonlinear impedance. Comparing this impedance with that of the surrounding environment across different frequencies helps clarify the device's behavior. Specifically, the total equivalent impedance of the device is determined by noting that the graphene pattern impedance is arranged in parallel with the spacer impedance. Here, the spacer impedance is purely imaginary, while the impedance of the graphene pattern includes both real and imaginary components. So, the following equations can be developed as Equation (4) [11].

$$\begin{aligned} Z_1 &= Z_{d1}\frac{Z_{AU} + jZ_{d1}\tan(\beta_{Aerogel} \times h_{Aerogel})}{Z_{d1} + jZ_{AU}\tan(\beta_{Aerogel} \times h_{Aerogel})} \\ Z_{AU} &= 0 \& Z_{d1} = \frac{Z_0}{n_{Aerogel}} \\ Z_1 &= jZ_{d1}\tan(\beta_{Aerogel} \times h_{Aerogel}) \\ Z_{eq} &= Z_{graphene} \,||\, Z_1 = \frac{Z_{graphene} \times Z_1}{Z_{graphene} + Z_1} \end{aligned} \tag{4}$$

The core principle of impedance matching is that maximum power transfer is achieved when the impedances on both sides are equal. Similarly, optimal wave absorption occurs when the device's impedance aligns with that of its surrounding environment. In free space, this equivalent impedance is typically 120 π Ω, though it can change depending on the particles present. This is an important consideration, as the structure is highly responsive to changes in the refractive index of its environment. Therefore, the operation of the proposed device can be explained through the impedance matching theorem [11].

A comprehensive approach has been adopted to obtain the reflection and phase profile at the target spectrum of 0.8 THz. To satisfy the required reflection and phase modulation for creating two different holograms, we achieved the following parameters shown in Figure 1(a) and (b): $P = 22$ μm, $d = 8$ μm, $h = 12$ μm, and $hi = 18$ μm. Also, graphene's Fermi level, μc, and its thickness were considered to be 0.1 eV and 0.34 nm, respectively. We applied the Pancharatnam–Berry technique to achieve the required phase shifts through adjustments in the geometrical orientation of the elements, as illustrated in Figure 1(d).

The metasurface design uses an ECM assuming linear impedance, which neglects nonlinear effects from carrier saturation, temperature changes, and strong THz fields. These nonlinearities can shift resonance and affect holographic performance, reducing model accuracy. While FDTD captures some nonlinearities, they are not fully addressed. Future improvements should include nonlinear circuit elements or experimental data to enhance real-time modeling and ensure robust, high-performance THz holography under varying power and temperature conditions [17, 18].

Here, we designed two types of holograms operating at two different temperatures to create holographic images at distances of 15 and 20 mm, respectively. The phase profiles of the holograms were obtained using a customized Gerchberg–Saxton algorithm [19, 20]. This algorithm relies on the transmission of light between two distinct planes, referred to as the hologram plane and the holographic image plane. Here, we designed a metasurface with a square size of 7 × 7 mm^2. Figure 3 illustrates the chosen images, simulated holograms, and the obtained phase profiles. It is useful to mention that the phase profile was translated to the distinguished unit cell orientation using the points shown in Figure 1(d).

3. Results and Discussion

The paper employs Floquet-port boundary conditions, which are exploited to achieve the metasurface structure. Floquet port is exclusively used with planar-periodic structures, where the unit

Figure 3
Hologram designs: (a, d) target images, (d, e) the simulated images, and (c, f) the obtained phase profiles

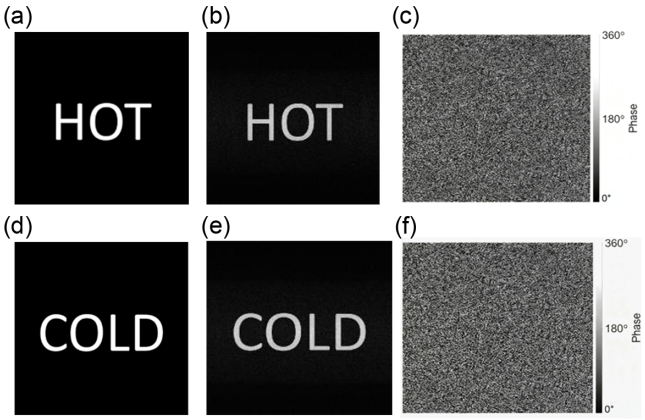

cells are defined in the x and y directions and vacuum space in the z-direction. In the z-axis, a perfectly matched layer (PML) guarantees no scattering, ensuring accurate results. The infinite structure is analyzed by studying a unit cell. Linked boundaries usually form the unit cell's sidewalls, but a boundary condition is required to account for the infinite space above. The Floquet port is designed for this purpose. Boundaries adjacent to a Floquet port must be linked boundaries. To achieve the desired simulation accuracy, we select the tetrahedral mesh type with adaptive mesh refinement, subdividing the structure into a large number of tetrahedrons. To ensure zero transmission, we use a gold dispersive medium with a thickness larger than the THz penetration depth.

In this work, the same computer Core i7@512 RAM is used for both the ECM and FDTD simulations. As simulation results, the FDTD method takes about 4 hours to complete, while the ECM development via MATLAM Mfile can generate results in less than a few seconds (3.4 s).

It should be noted that a genetic algorithm, along with the ECM, has been employed to ensure that the reflection of the structure does not decrease at the target spectrum of 0.8 THz. The simulated holographic images were obtained utilizing a FDTD method with PML boundary conditions. The excitation source was set using a Transverse Magnetic (TM) - polarized wave propagating along the long axis of the graphene ribbon. The normalized electromagnetic field at the holographic image planes is shown in Figure 4. Clearly, the proposed structure has the capability of creating the encoded information at the designed distance.

Figure 5 presents a systematic study on the impact of varying the Fermi level of the graphene layer on reflection and phase profiles. As the Fermi level deviates from the designed nominal

Figure 4
Results of FDTD simulation of the generated holograms when (a) the aerogel is at room temperature and (b) the aerogel is heated up

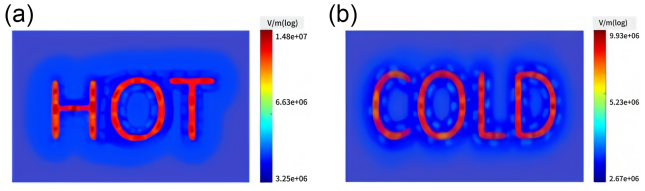

Figure 5
Reflection and phase modulation obtained at different graphene Fermi levels for the structure with aerogel thickness of (a) h and (b) hi. The dashed lines are interpolations of the data

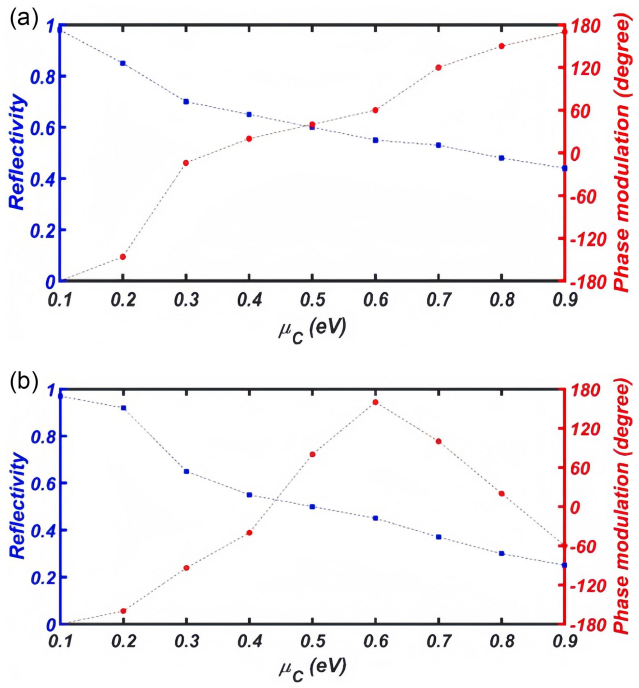

value, the reflection decreases. This reduction in reflectivity is still sufficient to provide the necessary intensity for image creation. However, the phase modulation is highly sensitive to changes in the Fermi level, which prevents the formation of holographic images. Consequently, the proposed device's high sensitivity to the graphene Fermi level can be leveraged for various applications that exploit this sensitivity. In this study, it is notable that the dynamic response of the holograms is achieved by maintaining a fixed Fermi level in the graphene and modulating the humidity, rather than by varying the graphene's Fermi level directly.

The temperature change required to achieve two-state holograms depends on the specific combination of aerogel materials used [21, 22]. The proposed structure can be implemented with an aerogel/PDMS (polydimethylsiloxane) nanocomposite, formed by incorporating aerogel into PDMS to produce a solution sensitive to temperature fluctuations [23]. Notably, the thickness of this material can be precisely adjusted by controlling the aerogel-to-PDMS ratio. Although the refractive index of this temperature-sensitive film changes slightly with temperature, this variation does not impact the device's performance. This is because the designed device achieves phase modulation through the Pancharatnam–Berry technique.

THz hologram generation offers numerous advantages and has a wide range of applications in various fields. One of the primary benefits is its ability to achieve high-resolution imaging and precise control over electromagnetic wave manipulation, which is crucial for advanced sensing and imaging technologies. THz holography can penetrate a variety of non-conductive materials, making it invaluable for nondestructive testing and inspection in industries including but not limited to aerospace, manufacturing, and cultural heritage preservation. Additionally, the non-ionizing nature of THz radiation ensures safe interactions with biological tissues, enabling medical imaging and security screening

applications. The high sensitivity and tunability of THz holographic systems also allow for dynamic reconfiguration, which is essential for adaptive optics, data encoding, and secure communication [24, 25].

4. Conclusion

This study presents the design of a dynamically tunable THz metasurface for reconfigurable holography by integrating temperature-responsive aerogel spacers with graphene ribbon elements and employing circuit-based modeling grounded in transmission line theory. The equivalent circuit model accurately predicts electromagnetic behavior, enabling efficient optimization while reducing reliance on full-wave simulations. Using the Pancharatnam–Berry phase, the metasurface achieves precise phase control, demonstrated through high-fidelity holographic image reconstruction at two distinct temperatures. Full-wave FDTD simulations validate the approach, while analysis of graphene's chemical potential highlights complementary electrical tunability. The proposed method offers scalable, low-cost, and lightweight reconfigurability through thermal actuation, with advantages including enhanced tunability, noninvasive control, and fabrication compatibility. Compared to electrical gating or phase-change materials, this introduces a novel thermal tuning pathway, though slower response times and aerogel handling challenges remain limitations. The work lays a foundation for multifunctional THz holography by suggesting integration of multi-channel tuning, nonlinear effects, and robust materials.

Ethical Statement

This study does not contain any studies with human or animal subjects performed by any of the authors.

Conflicts of Interest

The authors declare that they have no conflicts of interest to this work.

Data Availability Statement

Data are available from the corresponding author upon reasonable request.

Author Contribution Statement

Alireza Barati Haghverdi: Software, Resources. **Amir Ali Mohammad Khani:** Validation, Investigation, Visualization. **Ilghar Rezaei:** Methodology, Formal analysis. **Ali Soldoozy:** Conceptualization, Data curation. **Toktam Aghaee:** Writing – original draft, Writing – review & editing, Supervision, Project administration.

References

1. Nehzati, M., Haghverdi, A. B., Khani, A. A. M., Rezaei, I., & Aghaee, T. (2025). Wearable graphene-patterned gas detection sensor. *Results in Optics*, *21*, 100876. https://doi.org/10.1016/j.rio.2025.100876
2. Khani, A. A. M., Haghverdi, A. B., Rezaei, I., Zoljalali, S. J. H., & Aghaee, T. (2024). Tunable graphene-based wave absorber: Combined electrical and mechanical tuning. *Smart Wearable Technology. Advance online publication.* https://doi.org/10.47852/bonviewSWT52025851
3. Khani, A. A. M., Haghverdi, A. B., Rezaei, I., Soldoozy, A., & Aghaee, T. (2025). Hydrogel-based THz wave absorber. *Results in Optics*, *19*, 100810. https://doi.org/10.1016/j.rio.2025.100810
4. Huang, W., Li, C., Fang, B., Xu, J., Liu, F., Xu, L., . . . , & Jing, X. (2024). Research progress of terahertz wave dynamic control of digital coded metasurfaces. *Optics and Lasers in Engineering*, *174*, 107977. https://doi.org/10.1016/j.optlaseng.2023.107977
5. Fu, X., Wang, P., Liu, Y., Fu, Y., Cai, Q., Wang, Y., . . . , & Cui, T. J. (2025). Fundamentals and applications of millimeter-wave and terahertz programmable metasurfaces. *Journal of Materiomics*, *11*(1), 100904. https://doi.org/10.1016/j.jmat.2024.06.001
6. Fang, Z., Dong, W., Zhang, Z., Chen, R., He, J., & Chen, M. (2025). Tunable metasurface with dual-phase-change materials enables dynamic multi-image switching and encryption. *Physica B: Condensed Matter*, *716*, 417732. https://doi.org/10.1016/j.physb.2025.417732
7. Du, Z., He, C., Xin, J., & Song, Z. (2023). Terahertz dynamic multichannel holograms generated by spin-multiplexing reflective metasurface. *Optics Express*, *32*(1), 248–259. https://doi.org/10.1364/OE.510046
8. Haleem, A., Javaid, M., & Khan, I. H. (2020). Holography applications toward medical field: An overview. *Indian Journal of Radiology And Imaging*, *30*(03), 354–361. https://doi.org/10.4103/ijri.IJRI_39_20
9. Dong, B., Zhao, R., Wei, Q., Lu, X., Huang, W., Wang, J., . . . , & Huang, L. (2022). Terahertz switchable VO_2-Au hybrid active metasurface holographic encryption. *Optics Express*, *30*(12), 20750–20761. https://doi.org/10.1364/OE.461424
10. Rezaei, I., & Aghaee, T. (2025). Dual-bias graphene ring-based THz absorber: Wearable optical sensor. *IET Wireless Sensor Systems*, *15*(1), e70010. https://doi.org/10.1049/wss2.70010
11. Khavasi, A., & Rejaei, B. (2014). Analytical modeling of graphene ribbons as optical circuit elements. *IEEE Journal of Quantum Electronics*, *50*(6), 397–403. https://doi.org/10.1109/JQE.2014.2316133
12. Rezaei, I., Haghverdi, A. B., Soldoozy, A., Aghaee, T., & Biabanifard, S. (2024). Wearable Kapton graphene biosensor for detection of toxic gases. *Journal of Hazardous Materials Advances*, *15*, 100452. https://doi.org/10.1016/j.hazadv.2024.100452
13. Biabanifard, M., Asgari, S., Biabanifard, S., & Abrishamian, M. S. (2019). Analytical design of tunable multi-band terahertz absorber composed of graphene disks. *Optik*, *182*, 433–442. https://doi.org/10.1016/j.ijleo.2019.01.068
14. Han, S., Jiao, F., Khan, Z. U., Edberg, J., Fabiano, S., & Crispin, X. (2017). Thermoelectric polymer aerogels for pressure–temperature sensing applications. *Advanced Functional Materials*, *27*(44), 1703549. https://doi.org/10.1002/adfm.201703549
15. Wu, J., Fan, X., Liu, X., Ji, X., Shi, X., Wu, W., . . . , & Liang, J. (2022). Highly sensitive temperature–pressure bimodal aerogel with stimulus discriminability for human physiological monitoring. *Nano Letters*, *22*(11), 4459–4467. https://doi.org/10.1021/acs.nanolett.2c01145
16. Huang, G., Wu, D., Luo, J., Lu, L., Li, F., Shen, Y., & Li, Z. (2020). Generalizing the Gerchberg–Saxton algorithm for retrieving complex optical transmission matrices. *Photonics Research*, *9*(1), 34–42. https://doi.org/10.1364/PRJ.406010

17. Liang, G., Hu, X., Yu, X., Shen, Y., Li, L. H., Davies, A. G., . . . , & Wang, Q. J. (2015). Integrated terahertz graphene modulator with 100% modulation depth. *ACS Photonics*, *2*(11), 1559–1566. https://doi.org/10.1021/acsphotonics.5b00317
18. Wu, B., Liu, X., Liu, M., Fu, G., & Liu, Z. (2023). Thermally-electrically tunable coherent terahertz perfect absorber. *IEEE Photonics Technology Letters*, *35*(13), 709–712. https://doi.org/10.1109/LPT.2023.3274232
19. Zeng, D., Zong, S., Liu, G., Yuan, W., Liu, X., & Liu, Z. (2022). Dynamically electrical/thermal-tunable perfect absorber for a high-performance terahertz modulation. *Optics Express*, *30*(22), 39736–39746. https://doi.org/10.1364/OE.474970
20. Wu, S., Ladani, R. B., Zhang, J., Ghorbani, K., Zhang, X., Mouritz, A. P., . . . & Wang, C. H. (2016). Strain sensors with adjustable sensitivity by tailoring the microstructure of graphene aerogel/PDMS nanocomposites. *ACS Applied Materials & Interfaces*, *8*(37), 24853–24861. https://doi.org/10.1021/acsami.6b06012
21. Han, S., Jiao, F., Khan, Z. U., Edberg, J., Fabiano, S., & Crispin, X. (2017). Thermoelectric polymer aerogels for pressure–temperature sensing applications. *Advanced Functional Materials*, *27*(44), 1703549. https://doi.org/10.1002/adfm.201703549
22. Cyrus, S., & Biabanifard, S. (2021). Graphene-based THz absorber: adjustability via multiple gate biasing. *Heliyon*, *7*(7), e07633. https://doi.org/10.1016/j.heliyon.2021.e07633
23. Soltani-Zanjani, M., Biabanifard, S., Hemmatiyengejeh, S., Soltani, M., & Sadrnia, H. (2021). Multi-bias graphene-based THz super absorber. *Results in Physics*, *25*, 104326. https://doi.org/10.1016/j.rinp.2021.104326
24. Alagheband, M., Zhang, Q., & Jung, S. (2025). Accelerated creep prediction in 3D printed PETG components using the Stepped Iso-stress method. *Engineering Failure Analysis*, *182*, 110120. https://doi.org/10.1016/j.engfailanal.2025.110120
25. Alagheband, M., Kosarimovahhed, M., Zhang, Q., & Jung, S. (2025). Creep and failure of 3D-printed polymers: Impact of infill patterns and densities on shear strain and strength. *Engineering Failure Analysis*, *175*, 109568. https://doi.org/10.1016/j.engfailanal.2025.109568

How to Cite: Haghverdi, A. B., Khani, A. A.M., Rezaei, I., Soldoozy, A., & Aghaee, T. (2025). Dynamic THz Hologram Generation via Temperature-Tunable Aerogel-Spacer Graphene Metasurfaces for Sensing Applications. *Smart Wearable Technology*. https://doi.org/10.47852/bonviewSWT52027122